Received: 29 October 2021 | Revised: 25 February 2022 | Accepted: 19 March 2022

DOI: 10.1002/biot.202100583

Biotechnology Journal

RESEARCH ARTICLE

GFP-tagging of extracellular vesicles for rapid process development

Braulio Carrillo Sanchez[1] | **Matthew Hinchliffe**[2] | **Daniel G. Bracewell**[1]

[1]Department of Biochemical Engineering, University College London, London, United Kingdom

[2]UCB Pharma, Slough, Berkshire, United Kingdom

Correspondence
Daniel G. Bracewell, Department of Biochemical Engineering, University College London, London, UK.
Email: d.bracewell@ucl.ac.uk

Abstract

Extracellular vesicles (EVs) act as nano-scale molecular messengers owing to their capacity to shuttle functional macromolecular cargo between cells. This intrinsic ability to deliver bioactive cargo has sparked great interest in the use of EVs as novel therapeutic delivery vehicles; investments totaling over $2 billion in 2020 alone were reported for therapeutic EVs.

One of the bottlenecks facing the production of EVs is the lack of rapid and high throughput analytics to aid process development. Here CHO cells have been designed and engineered to express GFP-tagged EVs via fusion to CD81. Moreover, this study highlights the importance of parent cell characterization to ensure lack of non-fused GFP for the effective use of this quantitative approach. The fluorescent nature of resulting vesicles allowed for rapid quantification of concentration and yield across the EV purification process. In this manner, the degree of product loss was deduced by mass balance analysis of ultrafiltration processing, reconciled up to 97% of initial feed mass. The use of GFP-tagging allowed for straightforward monitoring of vesicle elution from chromatography separations and detection via western blotting. Collectively, this work illustrates the utility of GFP-tagged EVs as a quantitative and accessible tool for accelerated process development.

KEYWORDS
CHO cells, extracellular vesicles, nanobiotechnology, process analytics, process development, size exclusion chromatography, ultrafiltration

1 | INTRODUCTION

Extracellular vesicles (EVs) have become established as key mediators of intercellular communication and are secreted by virtually all cell types.[1] The umbrella term EVs comprises several types of lipid-bilayer enclosed vesicles with similar structural, biochemical, and functional properties. The two major vesicle populations of therapeutic interest include (1) small EVs/exosomes (40–150 nm size) that are derived through an endosomal route of biogenesis and (2) microvesicles (100–1000 nm) which are produced by the outward budding of the parent cell plasma membrane (Figure 1A). Additionally, cells undergoing programmed cell death by apoptosis are known to shed a third vesicle subtype known as apoptotic bodies with broad size ranges between 50 nm and 5 μm.[1–3] The significance of EVs as molecular messengers lies in

Abbreviations: CCM, clarified conditioned medium; CHO, Chinese hamster ovary; EVs, extracellular vesicles; GFP, green fluorescent protein; MWCO, molecular weight cut-off; NTA, nanoparticle tracking analysis; SEC, size exclusion chromatography; UF, ultrafiltration; cP, centipoise

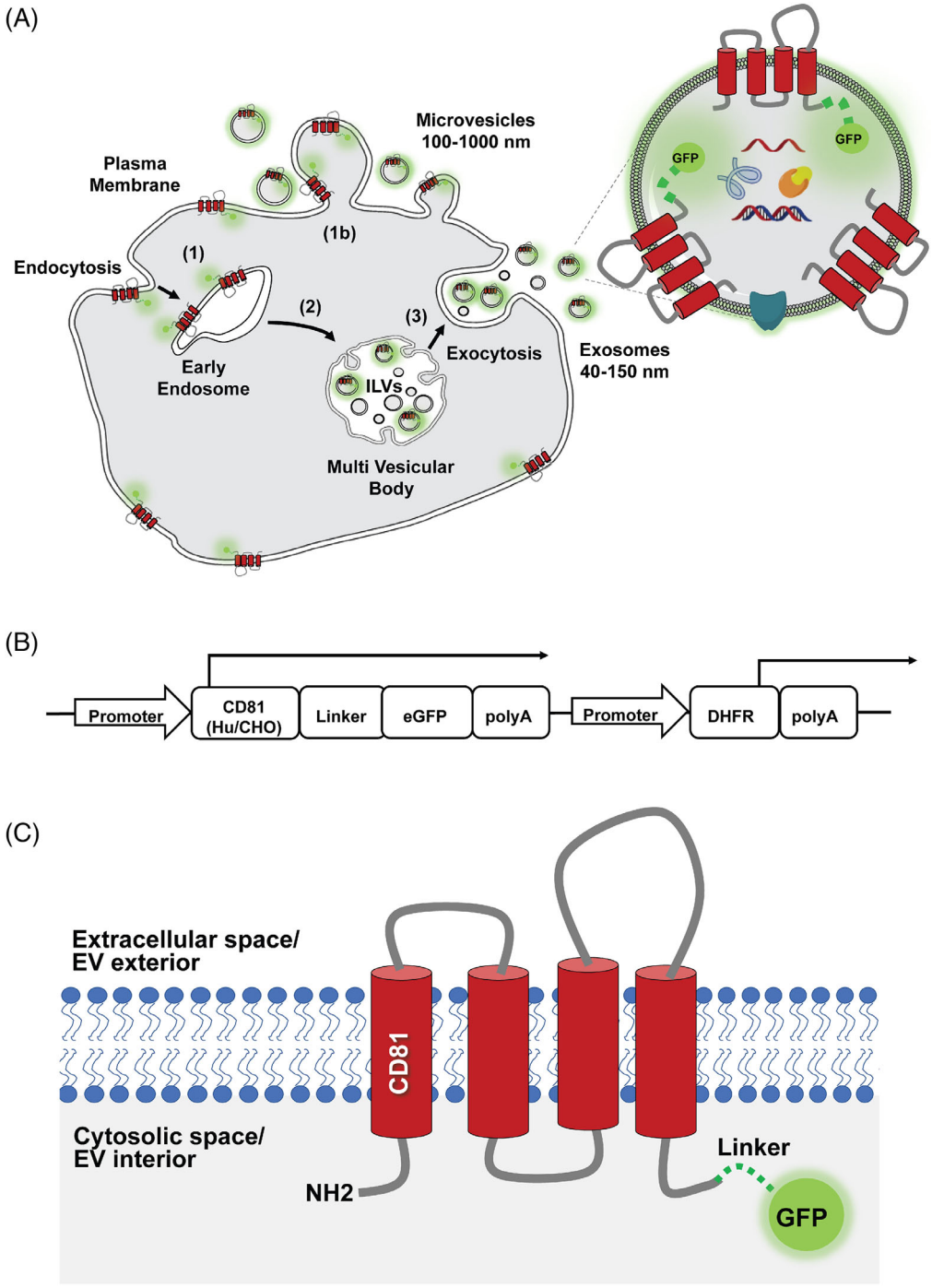

FIGURE 1 **(A)** EV biogenesis pathways leading to insertion of CD81-GFP within vesicles. (1) Early endosomes are formed by endocytosis. (2) Early endosomes mature into the multivesicular body (MVB). Inward budding of the membrane produces intraluminal vesicles (ILVs). (3) MVB fusion with plasma membrane releases ILVs from the cell. (1b) Microvesicles are formed by outward budding of plasma membrane. **(B)** Expression vector map for stable expression of CD81-GFP. **(C)** Schematic illustration of CD81-GFP topology within the lipid bilayer of cells and EVs

their ability to shuttle molecular cargo that has functional impact on recipient cells, particularly through nucleic acid delivery.[4] In recent years EVs have captured the growing attention of many biotechnology firms owing to their promising therapeutic potential.[5] This has resulted in increasingly lucrative investments to develop EV-mediated technologies; deals amounting to over $2 billion were reported in the year 2020.[6] Additionally, there is growing evidence that EVs could serve as non-invasive diagnostic tools to aid in early detection of disease, particularly cancers,[7,8] thus showcasing the diversity of EV research potential.

Currently, there is a lack of standardized methodology for the isolation of EVs. Ultracentrifugation (UC) is often the most commonly used isolation technique,[9] however, UC suffers from lack of scalability,[10] time efficiency and has been suggested to damage vesicles.[11] To

realize the therapeutic potential of EVs, production requires scalable methods for the processing of cell culture supernatant feed material. To address this, methods involving tangential flow filtration coupled with chromatography steps have been used effectively for isolation of EVs with scalable capabilities.[12–14] The tremendous interest in EVs in recent years has driven research into novel methods for analyzing these vesicles. However, many of these methods are lengthy and require highly specialized equipment, costly consumables or prelabelling steps.[15–19] Nanoparticle tracking analysis (NTA) remains amongst the most popular methods for routine EV quantification[9] despite known concerns relating to biased results depending on sample dilution and preparation.[20] Previous work has described the use of CD63 tetraspanin for GFP-EV tagging strategies in a transient manner allowing expanded analytical capacities for single vesicle characterization with higher vesicle specificity.[21] Similarly, CD63 has been tagged with luciferase via genetic fusion for EV detection and in-vivo uptake studies.[22] While providing high sensitivity, a luciferase-tagging approach requires the use of expensive substrates to generate signals with a specified half-life and are best suited for bio-distribution studies. In a different approach, recombinant EVs (rEV) tagged with GFP via HIV-1 gag polyprotein have been proposed as potential biological reference material allowing for recovery characterization following spiking of samples with rEVs.[23]

Overall, past work has largely neglected the potential use of EV-tagging strategies as an analytic approach to streamline EV process development. In this study we have genetically engineered Chinese hamster ovary (CHO) cells for stable expression of the tetraspanin CD81 fused to GFP via a flexible peptide linker to generate tagged EVs. In this way we aimed to exploit the known abundance of tetraspanin proteins within EVs to label both exosomes and microvesicles with GFP destined for the lumen of secreted vesicles.

We demonstrate it is possible to deduce total mass yields via measured GFP-concentration across fractions of the EV isolation process. This quantitative approach simply requires use of plate readers with fluorescent measurement capabilities. As such, we propose the use of GFP-tagged vesicles as an accessible, rapid, and high-throughput approach to simplify EV process development at bench scale and beyond.

2 | EXPERIMENTAL SECTION

2.1 | Plasmid construction

The protein sequence for the Chinese hamster homolog of CD81 was obtained from CHO-K1 genome (2014) Assembly: GCF_000223135.1 (Beijing Genomics Institute). Human CD81 was obtained from Uniprot (accession number: **P60033)**. Plasmids encoding gene inserts for CD81-GFP (CHO) and CD81-GFP (Hu) were synthesized by ATUM (California, USA). CD81-GFP fusion gene inserts were subcloned into an in-house expression vector (UCB, Slough, UK) using standard laboratory cloning techniques. Final constructs were verified by sanger sequencing.

2.2 | Cell culture

CHO cells were cultivated in suspension with HyClone ActiSM chemically defined medium (Cytiva life sciences) supplemented with 6 mM L-Glutamine. Cells were seeded at 0.2×10^6 viable cells/ml and maintained in Erlenmeyer shake flasks (Corning) in shaking incubators at 37°C with 80% humidity and 7.5% CO_2. Cell viability and density was determined using Vi-Cell XR Instrument (Beckman Coulter).

2.3 | Transfections for stable expression

CHO DG44 host cells were cultured in CD-DG44 medium (Gibco, Thermo Fisher Scientific) supplemented with 6 mM L-Glutamine and Pluronic F-68 (Gibco, Thermo Fisher Scientific). For electroporation, the Amaxa Cell Line Nucleofector Kit V and Amaxa Nucleofector II device were used (Lonza Group) according to the manufacturer's protocol. Briefly, cells were electroporated with linearized plasmid DNA. For each construct a total of 10 independent transfection reactions were carried out and then pooled together into T-175 flasks. After 24 h the pooled culture was split into T-25 flasks and transferred into selective medium. The resulting cell pools were then adapted back into shaking culture.

2.4 | Fluorescence microscopy and flowcytometry

For fluorescence microscopy imaging, cell culture samples were taken from shake flasks and diluted in 1X Phosphate–Buffered Saline (PBS). Nuclear staining was carried out using NucBlue Live ReadyProbes (Hoechst 33342) according to manufacturer's instructions (Invitrogen, Thermo Fisher Scientific). A total of 30,000 cells per well were dispensed into 96-well plates and images were acquired using the ImageXpress system (Molecular Devices) under FITC (Ex482, Em536) and DAPI (Ex377, Em447) channels. GFP flow cytometry analysis of cells was performed on the BD FACS Aria III system (BD Biosciences) under FITC channel.

2.5 | EV harvest

Stable cells expressing CD81-GFP (CHO) or CD81-GFP (Hu) were cultivated under batch culture conditions in 250 ml Erlenmeyer flasks. Cultures were terminated on day 5 and the conditioned medium was harvested. Cell culture supernatant was collected by $500 \times g$ centrifugation and then passed through 0.2 μm filters (Steriflip, Merck Millipore). 20 ml of the resulting clarified conditioned medium (CCM) was processed with 300 kDa Vivaspin 20 Ultrafiltration Units (Sartorius) according to manufacturer's protocol and retentates were concentrated to approximately 0.5 ml. Size exclusion chromatography (SEC) was performed using qEV original/35 nm (Izon Science) columns according to the manufacturer's protocol. Briefly, 0.4 ml of ultrafiltration retentate was loaded onto the columns and 0.5 ml fractions were

manually collected over a total elution run of 12 ml using PBS (10 mM, pH 7.4) as the buffer. Total protein was quantified with the Micro BCA Protein Assay Kit (Cat. 23235, Thermo Scientific) according to manufacturer's instructions.

2.6 | Fluorescence intensity quantification

GFP concentration in samples was estimated based on fluorescence intensity using Abcam GFP Quantification Kit (ab235672) according manufacturer's guidelines. For the purposes of this study, the optional GFP quenching solution included in the kit was omitted. Briefly, recombinant GFP standards and unknown samples were diluted using the included GFP assay buffer. GFP standard curves were prepared between range of 80–400 ng GFP/well (Supp Figure S1A) and 8–40 ng GFP/well (Supp Figure S1B). All samples were assayed in a final volume of 100 μl and fluorescence was measured using Ex = 485/20 nm, Em = 528/20 nm filter-set on Biotek Synergy2 microplate reader. Assays were carried out in black 96 well assay plates with clear flat bottom (Cat. 3603. Costar, Corning) to reduce inter-well interference.

2.7 | Nanoparticle tracking analysis

Particle concentration and size distributions were measured using the Nanosight NS300 equipped with Blue488 nm laser module and sCMOS camera. Samples were diluted to appropriate range and loaded into the low volume fluidic chamber using the NanoSight syringe pump. Camera frames were manually focused, and triplicate measurements were captured for 120 s at 25 frames per seconds. Instrument temperature was maintained at 25°C and sample viscosity set to 1.0 centipoise (cP). Resulting videos were processed at threshold level 5 on NTA software 3.3.

2.8 | Western blotting

Whole cell lysates were prepared on ice using RIPA lysis buffer (Thermo Scientific) and treated with 1X Protease Inhibitor Cocktail (Thermo Scientific). Total protein was quantified using micro BCA assay. Samples were prepared by mixing with 4X NuPAGE LDS Sample buffer at 1:3 ratio and then heated to 70°C. Samples were loaded onto 4%–12%, Bis-Tris, 1.5 mm gels alongside a reference protein ladder (26634, Invitrogen). Electrophoresis was run at 180 V with 1X MES SDS running buffer (Invitrogen, Thermo Scientific). Proteins were transferred to 0.45 μm PVDF membranes (Invitrogen, Thermo Scientific) with 1X Towbin buffer at 100 V for 75 min and blocked for 1 h. Blots were incubated overnight at 4°C with primary antibodies (1:1000 anti-GFP, MA5-15256, Invitrogen; 1:100 anti-CYC1, sc-514435, Santa Cruz). Membranes were incubated with polyclonal secondary antibody (1:500, Ref: 31430, Invitrogen) for 1 h at room temperature. ECL substrate (Ref: 34095, Thermo Scientific) was added and blots were visualized under chemiluminescence using an Amersham Imager A600 (GE Healthcare Life Sciences).

3 | RESULTS AND DISCUSSION

Production of tagged EVs started with the generation of cells expressing constructs with GFP-cargo destined to be enriched in EVs. CHO cells were selected for this work owing to their genomic plasticity, ease of handling and ability to thrive in chemically defined medium formulations which streamline EV purification. Additionally, recent work has demonstrated the use of DG44 CHO cells as a source of biocompatible EVs containing recombinant therapeutic cargo.[24] As such, CHO cells could also be readily adopted in future for bioprocessing of therapeutic EVs.

3.1 | Molecular design for secretion of GFP-tagged EVs

The design of constructs (Figure 1B) for generating GFP-tagged EVs began with the use of either human (Hu) or Chinese hamster (CHO) derived CD81 sequences to compare effectiveness for exploiting the host-cell machinery during EV biogenesis in DG44 CHO cells.

The integral membrane protein CD81 of the tetraspanin family was selected for EV-tagging owing to its prolific use as a molecular marker of EV membrane identity.[25] The crystal structure and proposed topology of full-length CD81 within the plasma membrane has been previously described.[26] CD81 has both the N-terminus and C-terminus present on the cytosolic leaflet of the plasma membrane in cells, which in turn corresponds to the interior of EVs. For our molecular design we opted to fuse GFP at the C-terminus to minimize the possibility of aberrant membrane insertion during translation and membrane translocation (Figure 1C). Furthermore, expression of closely related tetraspanin CD63-GFP has been reported to have minimal impact on vesicle integrity and overall proteomic composition of resulting EVs analyzed by mass spectrometry.[21]

Cassettes encoding the human (Hu) or Chinese hamster (CHO) sequence of CD81 fused to GFP via a flexible peptide linker were inserted into an optimized expression vector for recombinant protein production in CHO cells; the design of this construct includes the gene for dihydrofolate reductase (DHFR) downstream from the insert (Figure 1B), an established and routine selection marker for DG44 CHO cell lines. This molecular design for constitutive over-expression of CD81-GFP at the parent cell membrane aimed to exploit the endogenous mechanisms of EV biogenesis pathways to tag both microvesicles and exosomes with GFP (Figure 1A,C).

Live cell fluorescence imaging revealed clusters of CD81-GFP, particularly in close proximity to the periphery of parent cells. In addition, an outline of the plasma membrane could also be observed, as anticipated for a transmembrane protein (Figure 2A). We hypothesize that observation of such distinct clusters of GFP may highlight stages of EV

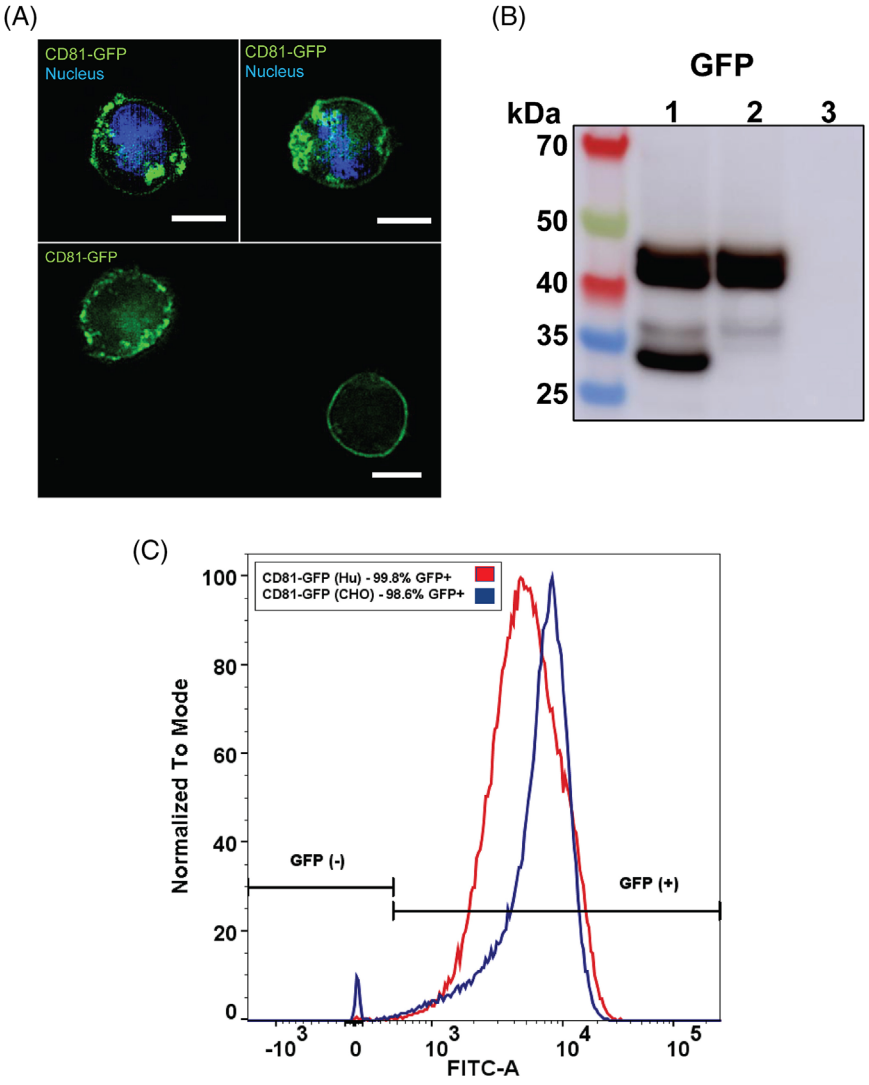

FIGURE 2 Expression Validation of CD81-GFP in parent cells. **(A)** Representative fluorescence microscopy imaging of live cells expressing CD81-GFP, indicating strong localisation along the plasma membrane. Scale bar represents 10 μm. **(B)** Anti-GFP western blot analysis of whole cell lysates to validate assembled GFP-fusion. Lanes: 1 CD81-GFP (Hu); 2 CD81-GFP (CHO); 3 negative control, lysate lacking expression of GFP. 30 μg protein loaded per lane. **(C)** CHO cell pools expressing CD81-GFP (Hu) and CD81-GFP (CHO) were analysed by flow cytometry after recovery from stable transfection. Histogram plots were normalised relative to the mode; event count values are represented as percentages of the modal count plotted against GFP FITC-A signal intensity

biogenesis (as outlined in Figure 1A) where CD81 becomes enriched in regions destined for cellular or vesicular trafficking. This observation requires further investigation into the cell biology of these processes however this is beyond the scope of this study. Expression of the CD81-GFP constructs was further validated by western blot analysis and flow cytometry (Figure 2B,C). Anti-GFP blot analysis indicated successful expression of full-length CD81-GFP fusion from parent cells expressing Human (Hu) and Hamster (CHO) tetraspanin sequences. However, we observed a substantial level of non-fused GFP detected from cells expressing human (Hu) CD81 homolog (Figure 2B, lane 1). The cause of this remains unclear considering the high degree of protein sequence identity (94.1%) across both homologs (Sup Figure S2) and identical C-terminal sequences where the linker-GFP is fused. This may be due to proteolytic cleaving at the linker/fusion point or the result of aberrant expression effectively producing free GFP.

To maximize the levels of GFP-tagged EVs recovered downstream, high proportions of parent cells expressing the protein of interest are desirable. To this end, flow cytometry studies indicated over 98% of cells to be GFP-positive within populations of stable transfected cells with both CD81-GFP (Hu) and (CHO) constructs (Figure 2C). Broader distribution of maximum GFP signal intensity was observed for parent cells expressing the CD81-GFP (Hu) construct (Figure 2C). We propose that this wider signal distribution may be the result of abundant non-fused GFP expression in accordance with western blot analysis discussed above (Figure 2B). Moreover, the identification of non-fused GFP expression highlights the potential underlying complexities that may arise from generating tagged EVs via protein fusions. Consequently, we later explored the implications of non-fused GFP when using GFP-tagged EVs as a quantification tool.

3.2 | Establishing cell culture & recovery of tagged EVs

Following the generation of stable cell pools that retained expression of CD81-GFP over multiple passages (data not shown), we then studied the potential use of GFP as a direct measure to track EV recovery across the EV purification process. In this study we established a

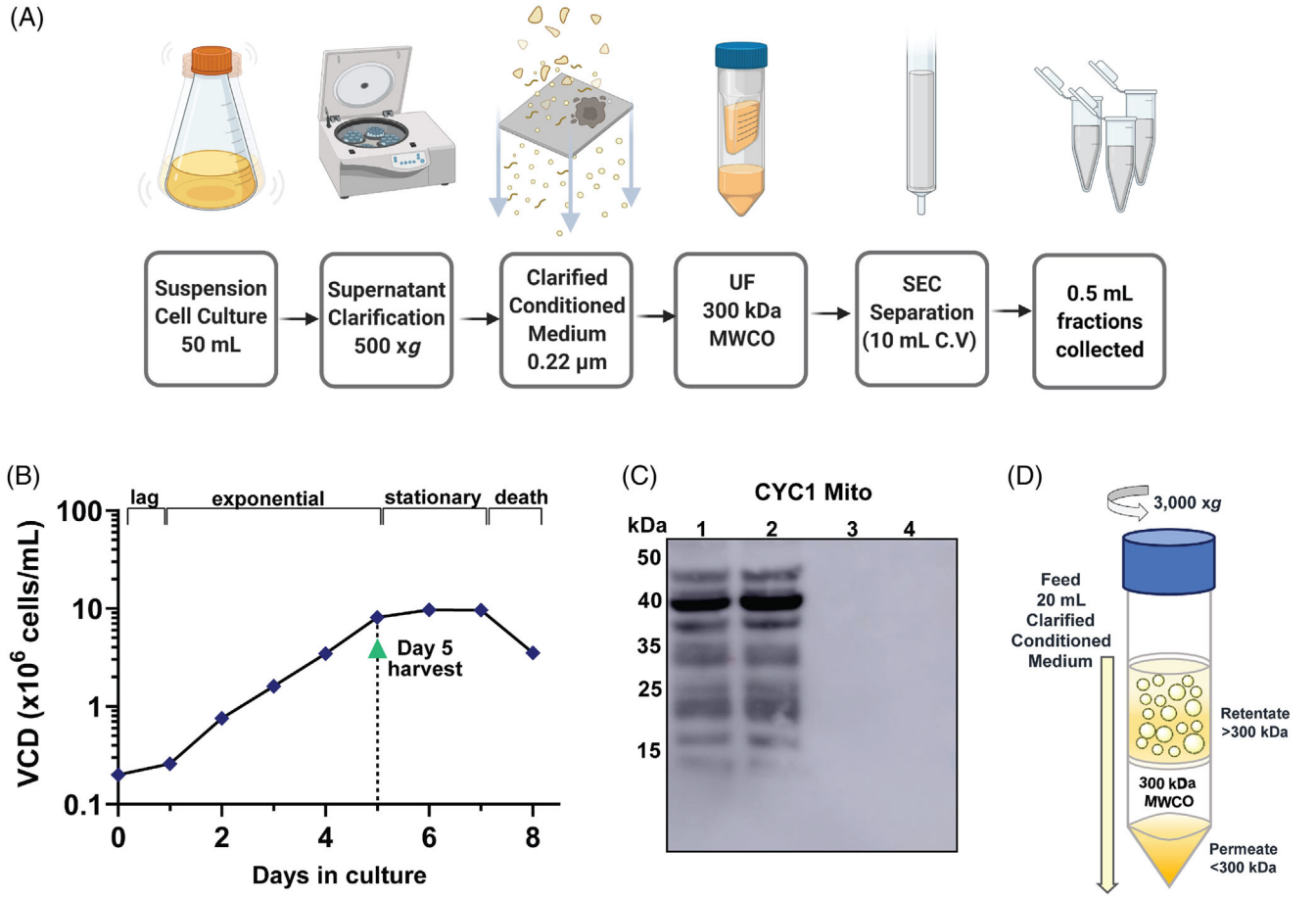

FIGURE 3 **(A)** Process outline for EV harvest from suspension batch culture. Graphic created with BioRender.com **(B)** Growth profile of CHO cells in suspension batch culture. Viable cell density (VCD) plotted against days in culture. Supernatant is harvested on day 5 where cells are approaching the end of exponential growth phase **(C)** Quality control western blot analysis of material harvested at Day 5 and Day 7 of cell culture. Blot was probed for Cytochrome c1 (CYC1), a common non-EV protein that may co-isolate with EVs. Lanes: 1 Day 7 cell lysate; 2 Day 5 cell lysates; 3 Day 7 UF retentate; 4 Day 5 UF retentate. 50 μg total protein loaded per well. **(D)** Schematic indicating bench-scale ultrafiltration process using 300 kDa molecular weight cut-off (MWCO)

bench-scale adaptation (Figure 3A) of emerging methods for scalable production of EVs[14,27,28] involving downstream processing steps such as clarification, ultrafiltration/diafiltration (UF/DF) and SEC.

For upstream cell culture we reasoned that maximal cell densities while retaining high viability of cells in would be most favorable for recovery of GFP-tagged EVs at bench scale, following the logic that a greater number of viable cells could yield a greater quantity of EVs. Retaining high viability is of great importance for isolation of high-quality EV preparations as this reduces the abundance of impurities such as apoptotic bodies that are released by cells undergoing apoptosis.[29,30] To establish a suitable point of culture harvest, we studied the growth profile of CHO cells across a total period of 8 days of cells in suspension batch culture (Figure 3B). Accordingly, culture of cells up to Day 5 allowed for routine harvest of cultures at viable cell densities at or above 7×10^6 viable cells/ml, corresponding to late-stage exponential phase of growth and therefore promoting a healthy population of parent cells.

The CCM collected from a harvest contains secreted EVs among other macromolecular impurities from the upstream cell culture process. Ultrafiltration processing has been widely incorporated into isolation processes[11,14,27,31] as a means of primary recovery to enrich EVs from CCM. Separation of macromolecules and EVs by ultrafiltration is based on the use of polymer membranes with specific molecular weight cut-off (MWCO) where EVs are expected to be retained in the sample retentate (Figure 3D) while smaller molecules pass through into the permeate waste. For this work we employed the use of bench scale of UF devices for the processing of CCM (Figure 3A,D) to concentrate EVs in the retentate up to 40-fold. CYC1 is a non-EV associated protein of mitochondrial origin. To assess the depletion of large cellular debris such as lysed mitochondria, UF retentates were subject to western blot analysis which confirmed a lack of CYC1 in our preparations as shown by absence of bands in lanes 3 and 4 (Figure 3C). Additionally, the absence of CYC1 is suggestive of EV preparations containing primarily small EVs such as exosomes.[25]

Particle analysis of UF EV material indicated comparable size distribution and particle titers between CD81-GFP(CHO) derived harvests and negative control material from cells lacking CD81-GFP construct expression. However, decreased overall particle titers were recovered

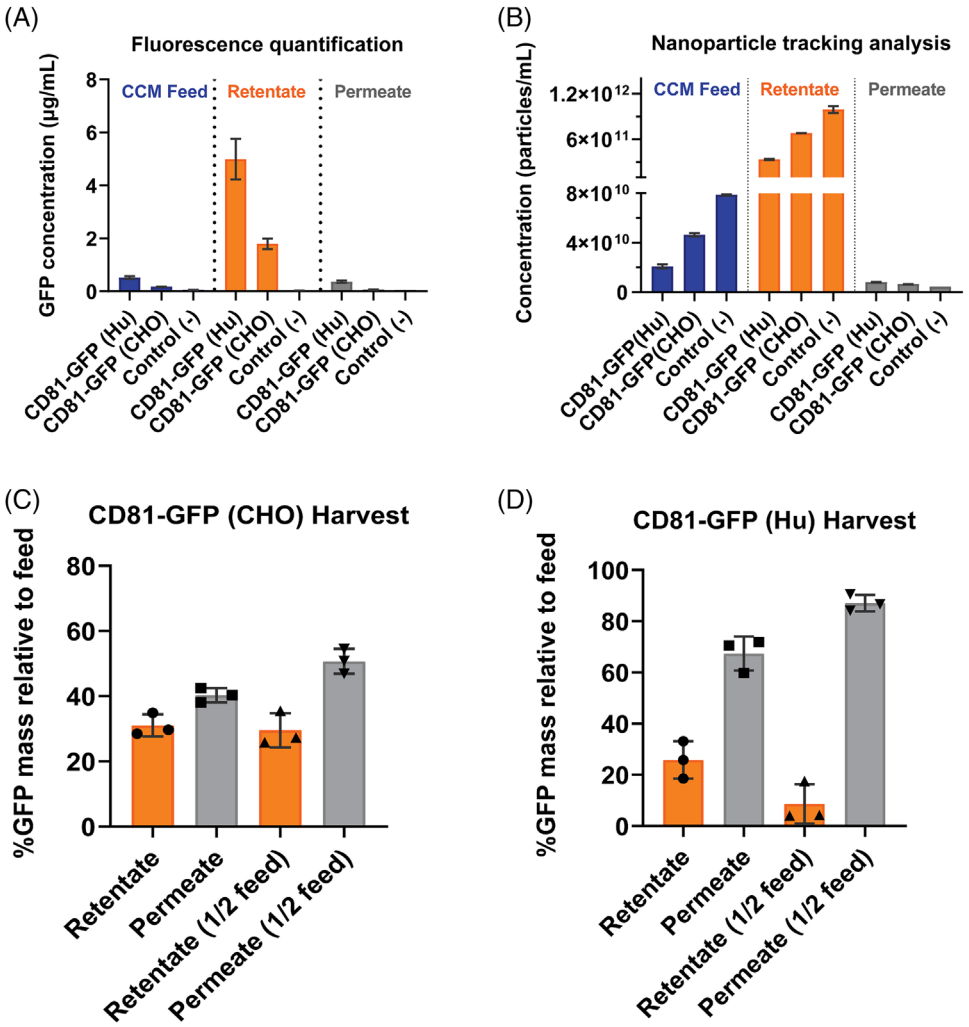

FIGURE 4 GFP-tagged EVs facilitate analysis of product recovery from ultrafiltration processing. **(A)** Fluorescence based quantification of GFP concentration in clarified conditioned medium (CCM) feed, retentate and permeate fractions. N = 7 feed; N = 9 retentate; N = 6 permeate. Error bars represent ± SD **(B)** NTA-based quantification of total particle concentration in material from UF fractions. N = 3 technical replicates, error bars represent ± SEM. **(C, D)** Evaluation of feed burden on GFP recovery. 20 mL of CCM feed material was loaded for full feed and 10 mL of feed was topped up with 10 mL PBS for ½ feed burden. Mass of GFP in UF fractions expressed as a percentage of total GFP mass in the initial feed material where feed = 100%. N = 3, error bars represent ± SD. N numbers indicate independent EV isolation replicates unless specified otherwise

from CD81-GFP(Hu) UF material, possibly linked to abundant free GFP expression (Supp Figure S3A,B).

3.3 | Characterization of ultrafiltration recovery

Fluorescence intensity was measured across the three fractions of the ultrafiltration process to evaluate the amount of GFP recovered in the retentate. It was possible to rapidly quantify GFP concentrations in the magnitude of μg/ml across CCM feed, retentate and permeate samples in 96-well plates from minimal sample volume of 100 μl.

A significant enrichment of GFP fluorescence signal was observed in the retentate fractions recovered from UF processing (Figure 4A). Moreover, fluorescence quantification revealed threefold greater GFP concentration in retentate material recovered from cells expressing CD81-GFP (Hu) compared to material from CD81-GFP (CHO) cells. Indeed, NTA concentration measurements also indicated EV enrichment in retentate material with particle counts in the magnitude of 10^{11} – 10^{12} particles/ml (Figure 4B). While NTA particle concentrations in retentates were higher in material from CD81-GFP (CHO) cells compared to CD81-GFP (Hu), the measured GFP concentration was significantly higher for CD81-GFP (Hu) retentates (Figure 4A). We propose this difference is likely caused by the expression of non-fused GFP from CD81-GFP (Hu) cells (Figure 2B) which is being held in the retentate despite the MWCO of 300 kDa being at least 10-fold larger than the molecular weight of GFP. This highlights the importance of ensuring that parent cells are not expressing free GFP which can lead to erroneous measurements if using this approach to estimate EV yield. Importantly, this also demonstrates further ambiguity that may arise if only a single method of EV quantification is used.

The GFP quantification strategy was then employed for mass balance analysis to generate approximations of total GFP mass present in

the CCM feed, retentate and permeate fractions. In these studies we explored the effect of feed bioburden on filtration recovery by loading UF devices with undiluted CCM feed or 1:2 diluted feed termed the 'half-feed'. In this manner we aimed to evaluate the impact of feed burden on GFP recovery from UF processing. Mass balance analysis of material derived from CD81-GFP (CHO) harvests indicated a total GFP yield of 40.3% in the permeate for full feed conditions. Under half-feed conditions, GFP yield in the permeate increased to 50.7% which indicates greater vesicle loss in the permeate under reduced burden on the filtration membrane (Figure 4C, Supp Table S1A,B). Interestingly, we did not observe a significant change in GFP yield (%) in the retentates derived from full or half-feed processing of CD81-GFP (CHO) material (Figure 4C).

To calculate the GFP mass assumed lost to the ultrafiltration membrane, the sum of GFP mass in the retentate and permeate was subtracted from the total GFP mass measured in the initial feed. Accordingly, 28.7% GFP yield was assumed as membrane loss for processing of CD81-GFP (CHO) full feed material. In contrast, half-feed processing resulted in reduced loss with 19.7% GFP yield attributed the membrane (Supp Table S1A,1B). Consequently, we reasoned that greater feed burden results in an increased membrane loss, likely due to cake layer formation; however, reducing feed burden results in a similar degree of loss but instead attributed to the permeate.

As discussed above, CD81-GFP (Hu) cells are liable to expressing detectable levels of non-fused GFP (Figure 2B) which would distort EV yield estimation. In mass balance analysis of material from these cells, we measured a loss of GFP yield (%) in retentate of over three-fold under half-feed conditions (Figure 4D, Supp Table S2A,B). This loss in GFP retentate yield could be the result decreased membrane fouling under half-feed conditions, allowing potential non-fused GFP aggregates in the retentate to pass through the membrane more readily.

Moreover, it should be advised that potential photobleaching of GFP could result in overestimation of product loss and samples should be carefully stored. Similarly, discrepancies in fluorescence intensity of free and conjugated GFP may result in altered recovery estimates.

3.4 | Tracking elution of GFP-EVs from SEC

The final step in our EV isolation process was SEC separation (Figure 3A) of UF retentate material harvested from CD81-GFP (CHO) and CD81-GFP (Hu) parental cell lines. Fractions of 0.5 ml were manually collected over a total elution volume of 12 ml and subjected to fluorescence quantification, total protein quantification and western blot analysis (Figure 5A-D).

GFP-fluorescence proved to be a rapid means of quantifying concentration of eluted GFP-tagged EVs even below 1 μg/ml. Moreover, samples were analyzed without prior treatment or lengthy incubation times. Despite significant sample dilution as a result of the SEC process, it was still possible to measure the fluorescence intensity of eluted fractions. GFP-tagged EVs were eluted between 3.5 and 4.0 ml which produced a major GFP-concentration peak in material from CD81-GFP (CHO) cells (Figure 5A). In agreement with this, anti-GFP western blot analysis of elution fractions indicated strong enrichment of CD81-GFP fusion in the EV elution fractions compared to UF material (Figure 5C). Total protein analysis indicated broader peaks corresponding to free protein impurity elution between 5.0 and 11.0 ml elution fractions (Figure 5A). NTA studies of the EV elution fractions (3.5–4.5 ml) indicated size particle size distributions in the expected range for EVs (Figure 5E) with mean particle sizes decreasing with greater elution volume, in agreement with larger vesicles eluting first (Supp Tables S3 and 4).

It is important to highlight that some fluorescence signal was measured between fractions 7–10 ml (Figure 5A). Initially, this suggested elution of free GFP from CD81-GFP (CHO) harvests. However, blotting indicated the absence of prominent GFP bands corresponding to these fractions (Figure 5C). Combined, this observation implies the measured fluorescence signal can be attributed to background fluorescence from substantial free proteins eluting between 7 and 10 ml. Accordingly, it cannot be fully excluded that intrinsic EV proteins may contribute low-level fluorescence signal. We propose future work could employ fluorescence plate-readers equipped with monochromators to best minimize non-specific background. One may also consider treatment of samples with commercial GFP quench solution (please see methods). On this occasion this treatment was excluded from our study as we aimed to maintain a simple and rapid approach to track elution.

On the contrary, elution of GFP-tagged EVs from CD81-GFP (Hu) cells produced only a minor GFP concentration peak between fractions 3.5 and 4.0 ml. Instead, a major GFP concentration peak corresponding to free protein elution was observed (Figure 5B). This observation confirmed that a significant level of non-fused GFP still remained in the UF retentate harvested from CD81-GFP (Hu) cells. Fluorescent proteins have a known propensity to dimerize non-covalently,[32,33] as such we speculate these observations could be caused an abundance of non-fused GFP aggregates. This notion was supported through western blot analysis indicating potential GFP aggregates eluting between 5.5 and 11.0 ml (Figure 5D). NTA analysis of UF material from CD81-GFP (Hu) cells prior to SEC separation show a greater variation in particle size distribution with multiple minor peaks, also suggestive of aggregate formation (Figure 5F).

Despite the substantial amounts of non-fused GFP in elution fractions, strong enrichment of correctly fused CD81-GFP bands can indeed be observed on the blot between 3.5 and 4.0 ml (Figure 5D). In this scenario, the value of fluorescence intensity as a direct measure of EV concentration is compromised by significant 'free' GFP molecules that distorts measurements starting at the feed material. Accordingly, our findings demonstrate that appropriate characterization of parent cell expression should be considered for effective EV monitoring with this analytical approach.

4 | SUMMARY

The purification challenges faced for the effective isolation of EVs are compounded by the lack of appropriate analytical techniques to better understand yield and recovery of an EV isolation process.

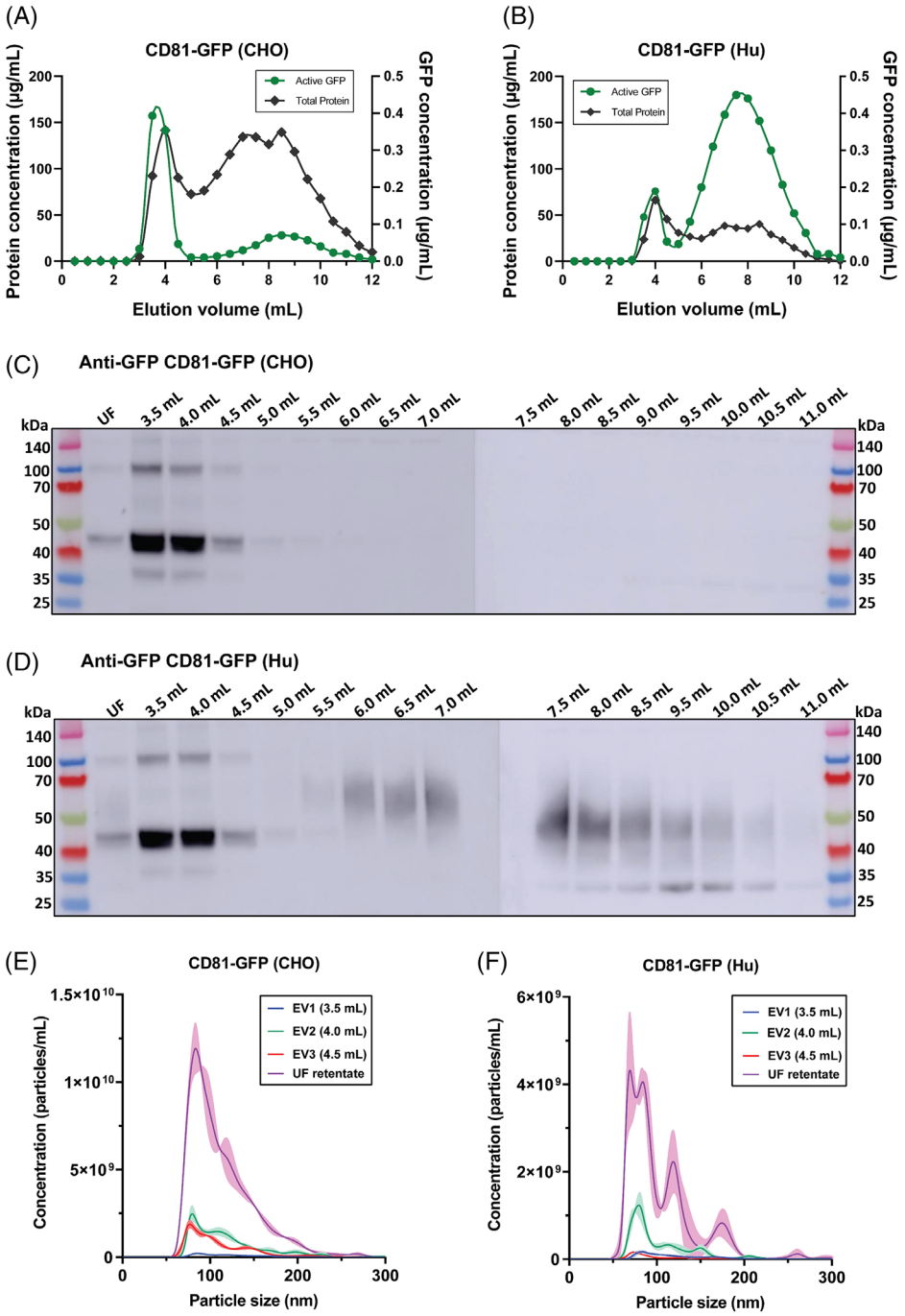

FIGURE 5 **(A, B)** Elution of extracellular vesicles from SEC separation tracked via GFP fluorescence signal. Void volume is expected between 0.0 mL – 3.0 mL, EV elution range is expected between 3.5 mL – 4.5 mL. Free protein is expected to elute after 4.5 mL. N = 3, mean values indicated. **(C, D)** Anti-GFP western blot analysis of elution fractions of SEC runs between 3.5 mL – 11.0 mL. 1 μg protein loaded per well. UF indicates ultrafiltration retentate. Fractions were analysed across two separate blots and developed images were stitched together using ImageJ software. **(D, E)** NTA Particle size distribution of UF retentate material and SEC fractions corresponding to vesicle elution (EV1, EV2, EV3). Shaded regions indicate ± SEM of three technical replicates. Supporting size and particle concentrations indicated in supplemental Tables S3 and S4. N numbers indicate independent EV isolation replicates unless specified otherwise

Accordingly, rapid and accessible analytical methods remain one of the greatest challenges also facing wider areas of research concerning EVs.[18] This is of particular importance for process development of EVs derived from cell culture supernatant. Total protein quantification methods such as bicinchoninic acid (BCA) assay are commonly combined with NTA, however, these require incubation times and are susceptible to interference from numerous substances including lipids and glucose[34,35] which are likely to be present in EV feed material and thus may significantly exaggerate results. The combination of total protein and total lipid quantification has been proposed as a metric for

evaluating quality of EVs.[36] As such, protein-lipid ratios provide an additional analytic to consider for assessing purity of EVs, perhaps as an end point analytic during process development. However, the disadvantage to this method lies in the use of limited reference standards such as fish oil and cholesterol which are unlikely to fully reflect the variety of lipids present in EV membranes.

In the present study we have proposed the potential use of GFP-tagged EVs derived from stable cell lines as a method for straightforward and rapid process characterization. Our findings through exploring this method revealed the need for further optimization of our own process, particularly to reduce losses while increasing retentate yields. We propose this could be explored further by employing the same fluorescence-based assays to evaluate performance of different membrane MWCO filters or membrane materials.

Importantly, we have highlighted that attention must be paid to ensure candidate cell lines do not display aberrant expressions of non-fused GFP in order to use this quantitative approach effectively. Through the comparison of EV material harvested from CD81-GFP (CHO) and CD81-GFP (Hu) cell lines, we were able to establish that CD81-GFP (CHO) cell lines do not secrete non-fused GFP above detectable levels; this is a critical attribute for a candidate cell line if GFP-EVs are to be used as a measure of EV recovery. If employed correctly with the suggested measures, the use of GFP-tagged EVs is time effective as samples can easily be analyzed in high-throughput formats using multi-well plates with minimal pre-treatment. Moving forward, the use of convenient dot-blotting techniques could be used in conjunction to reliably evaluate EV elution via the enclosed GFP-tag. Collectively, the flexibility afforded through this straightforward and rapid approach could be used by anyone to accelerate their characterization of an EV isolation process at any stage of development.

ACKNOWLEDGMENTS

Funding received from the UK Engineering & Physical Sciences Research Council (EPSRC) for the Centre for Doctoral Training in Emergent Macromolecular Therapies hosted at University College London (Grant Reference: EP/I033270/1).

CONFLICT OF INTEREST

None.

DATA AVAILABILITY STATEMENT

The data that supports the findings of this study are available in the supplementary material of this article.

ORCID

Braulio Carrillo Sanchez https://orcid.org/0000-0002-0063-1262

REFERENCES

1. Yáñez-Mó, M., Siljander, P. R. M., Andreu, Z., Zavec, A. B., Borràs, F. E., Buzas, E. I., Buzas, K., Casal, E., Cappello, F., Carvalho, J., Colás, E., Cordeiro-Da Silva, A., Fais, S., Falcon-Perez, J. M., Ghobrial, I. M., Giebel, B., Gimona, M., Graner, M., Gursel, I. … De Wever, O. (2015). Biological properties of extracellular vesicles and their physiological functions. *Journal of Extracellular Vesicles*, *4*(2015), 1–60. https://doi.org/10.3402/jev.v4.27066.
2. Willms, E., Johansson, H. J., Mäger, I., Lee, Y., Blomberg, K. E. M., Sadik, M., Alaarg, A., Smith, C. I. E., Lehtiö, J., El Andaloussi, S., Wood, M. J. A. & Vader, P. (2016). Cells release subpopulations of exosomes with distinct molecular and biological properties. *Science Reports*, *6*(March), 1–12. https://doi.org/10.1038/srep22519.
3. Jeppesen, D. K., Fenix, A. M., Franklin, J. L., Higginbotham, J. N., Zhang, Q., Zimmerman, L. J., Liebler, D. C., Ping, J., Liu, Q., Evans, R., Fissell, W. H., Patton, J. G., Rome, L. H., Burnette, D. T. & Coffey, R. J. (2019). Reassessment of exosome composition. *Cell*, *177*(2), 428–445.e18. https://doi.org/10.1016/j.cell.2019.02.029.
4. Valadi, H., Ekström, K., Bossios, A., Sjöstrand, M., Lee, J. J. & Lötvall, J. O. (2007). Exosome-mediated transfer of mRNAs and microRNAs is a novel mechanism of genetic exchange between cells. *Nature Cell Biology*, *9*(6), 654–659. https://doi.org/10.1038/ncb1596.
5. El Andaloussi, S., Mäger, I., Breakefield, X. O. & Wood, M. J. A. (2013). Extracellular vesicles: Biology and emerging therapeutic opportunities. *Nature Reviews Drug Discovery*, *12*(5), 347–357. https://doi.org/10.1038/nrd3978.
6. Zipkin, M. (2020). Big pharma buys into exosomes for drug delivery. *Nature Biotechnology*, *38*(11), 1226–1228. https://doi.org/10.1038/s41587-020-0725-7.
7. Welton, J. L., Brennan, P., Gurney, M., Webber, J. P., Spary, L. K., Carton, D. G., Falcón-Pérez, J. M., Walton, S. P., Mason, M. D., Tabi, Z. & Clayton, A. (2016). Proteomics analysis of vesicles isolated from plasma and urine of prostate cancer patients using a multiplex, aptamer-based protein array. *Journal of Extracellular Vesicles*, *5*(1), 1–18. https://doi.org/10.3402/jev.v5.31209.
8. Halvaei, S., Daryani, S., Eslami-S, Z., Samadi, T., Jafarbeik-Iravani, N., Bakhshayesh, T. O., Majidzadeh-A, K. & Esmaeili, R. (2018). Exosomes in cancer liquid biopsy: A focus on breast cancer. *Molecular Therapy – Nucleic Acids*, *10*(March), 131–141. https://doi.org/10.1016/j.omtn.2017.11.014.
9. Gardiner, C., Vizio, D. Di, Sahoo, S., Théry, C., Witwer, K. W., Wauben, M. & Hill, A. F. (2016). Techniques used for the isolation and characterization of extracellular vesicles: Results of a worldwide survey. *Journal of Extracellular Vesicles*, *5*(1). https://doi.org/10.3402/jev.v5.32945.
10. Paganini, C., Capasso Palmiero, U., Pocsfalvi, G., Touzet, N., Bongiovanni, A. & Arosio, P. (2019). Scalable production and isolation of extracellular vesicles: Available sources and lessons from current industrial bioprocesses. *Biotechnology Journal*, *14*(10), 1–10. https://doi.org/10.1002/biot.201800528.
11. Lobb, R. J., Becker, M., Wen, S. W., Wong, C. S. F., Wiegmans, A. P., Leimgruber, A. & Möller, A. (2015). Optimized exosome isolation protocol for cell culture supernatant and human plasma. *Journal of Extracellular Vesicles*, *4*(1), 1–11. https://doi.org/10.3402/jev.v4.27031.
12. Gazze, S. A., Thomas, S. J., Garcia-Parra, J., James, D. W., Rees, P., Marsh-Durban, V., Corteling, R., Gonzalez, D., Conlan, R. S. & Francis, L. W. (2021). High content, quantitative AFM analysis of the scalable biomechanical properties of extracellular vesicles. *Nanoscale*, *13*(12), 6129–6141. https://doi.org/10.1039/d0nr09235e.
13. Watson, D. C., Yung, B. C., Bergamaschi, C., Chowdhury, B., Bear, J., Stellas, D., Morales-Kastresana, A., Jones, J. C., Felber, B. K., Chen, X. & Pavlakis, G. N. (2018). Scalable, cGMP-compatible purification of extracellular vesicles carrying bioactive human heterodimeric IL-15/lactadherin complexes. *Journal of Extracellular Vesicles*, *7*(1). https://doi.org/10.1080/20013078.2018.1442088.
14. Nordin, J. Z., Lee, Y., Vader, P., Mäger, I., Johansson, H. J., Heusermann, W., Wiklander, O. P. B., Hällbrink, M., Seow, Y., Bultema, J. J., Gilthorpe, J., Davies, T., Fairchild, P. J., Gabrielsson, S., Meisner-Kober, N. C., Lehtiö, J., Smith, C. I. E., Wood, M. J. A. & Andaloussi, S. E. L. (2015). Ultrafiltration with size-exclusion liquid chromatography for high yield isolation of extracellular vesicles preserving intact biophysical and functional properties. *Nanomedicine: Nanotechnology, Biology,*

and Medicine, *11*(4), 879–883. https://doi.org/10.1016/j.nano.2015.01.003.
15. Gandham, S., Su, X., Wood, J., Nocera, A. L., Alli, S. C., Milane, L., Zimmerman, A., Amiji, M. & Ivanov, A. R. (2020). Technologies and standardization in research on extracellular vesicles. *Trends in Biotechnology*, *38*(10), 1066–1098. https://doi.org/10.1016/j.tibtech.2020.05.012.
16. Im, H., Shao, H., Park, Y. Il, Peterson, V. M., Castro, C. M., Weissleder, R. & Lee, H. (2014). Label-free detection and molecular profiling of exosomes with a nano-plasmonic sensor. *Nature Biotechnology*, *32*(5), 490–495. https://doi.org/10.1038/nbt.2886.
17. Tian, Y., Gong, M., Hu, Y., Liu, H., Zhang, W., Zhang, M., Hu, X., Aubert, D., Zhu, S., Wu, L. & Yan, X. (2020). Quality and efficiency assessment of six extracellular vesicle isolation methods by nano-flow cytometry. *Journal of Extracellular Vesicles*, *9*(1), 1697028. https://doi.org/10.1080/20013078.2019.1697028.
18. Lucchetti, D., Fattorossi, A. & Sgambato, A. (2019). Extracellular vesicles in oncology: Progress and pitfalls in the methods of isolation and analysis. *Biotechnology Journal*, *14*(1), 1–10. https://doi.org/10.1002/biot.201700716.
19. Simonsen, J. B. (2019). Pitfalls associated with lipophilic fluorophore staining of extracellular vesicles for uptake studies. *Journal of Extracellular Vesicles*, *8*(1). https://doi.org/10.1080/20013078.2019.1582237.
20. Gardiner, C., Ferreira, Y. J., Dragovic, R. A., Redman, C. W. G. & Sargent, I. L. (2013). Extracellular vesicle sizing and enumeration by nanoparticle tracking analysis. *Journal of Extracellular Vesicles*, *2*(1), 1–11. https://doi.org/10.3402/jev.v2i0.19671.
21. Corso, G., Heusermann, W., Trojer, D., Görgens, A., Steib, E., Voshol, J., Graff, A., Genoud, C., Lee, Y., Hean, J., Nordin, J. Z., Wiklander, O. P. B., El Andaloussi, S. & Meisner-Kober, N. (2019). Systematic characterization of extracellular vesicles sorting domains and quantification at the single molecule–single vesicle level by fluorescence correlation spectroscopy and single particle imaging. *Journal of Extracellular Vesicles*, *8*(1). https://doi.org/10.1080/20013078.2019.1663043.
22. Hikita, T., Miyata, M., Watanabe, R. & Oneyama, C. (2018). Sensitive and rapid quantification of exosomes by fusing luciferase to exosome marker proteins. *Science Reports*, *8*(1), 1–14. https://doi.org/10.1038/s41598-018-32535-7.
23. Geeurickx, E., Tulkens, J., Dhondt, B., Van Deun, J., Lippens, L., Vergauwen, G., Heyrman, E., De Sutter, D., Gevaert, K., Impens, F., Miinalainen, I., Van Bockstal, P. J., De Beer, T., Wauben, M. H. M., Nolte-'t-Hoen, E. N. M., Bloch, K., Swinnen, J. V., van der Pol, E., Nieuwland, R., … Hendrix, A. (2019). The generation and use of recombinant extracellular vesicles as biological reference material. *Nature Communication*, *10*(1), 1–12. https://doi.org/10.1038/s41467-019-11182-0.
24. Seras-Franzoso, J., Díaz-Riascos, Z. V., Corchero, J. L., González, P., García-Aranda, N., Mandaña, M., Riera, R., Boullosa, A., Mancilla, S., Grayston, A., Moltó-Abad, M., Garcia-Fruitós, E., Mendoza, R., Pintos-Morell, G., Albertazzi, L., Rosell, A., Casas, J., Villaverde, A., Schwartz, S. & Abasolo, I. (2021). Extracellular vesicles from recombinant cell factories improve the activity and efficacy of enzymes defective in lysosomal storage disorders. *Journal of Extracellular Vesicles*, *10*(5). https://doi.org/10.1002/jev2.12058.
25. Théry, C., Witwer, K. W., Aikawa, E., Alcaraz, M. J., Anderson, J. D., Andriantsitohaina, R., Antoniou, A., Arab, T., Archer, F., Atkin-Smith, G. K., Ayre, D. C., Bach, J. M., Bachurski, D., Baharvand, H., Balaj, L., Baldacchino, S., Bauer, N. N., Baxter, A. A., Bebawy, M., … & Zuba-Surma, E. K. (2018). Minimal information for studies of extracellular vesicles 2018 (MISEV2018): a position statement of the International Society for Extracellular Vesicles and update of the MISEV2014 guidelines. *Journal of Extracellular Vesicles*, *7*(1). https://doi.org/10.1080/20013078.2018.1535750.
26. Zimmerman, B., Kelly, B., McMillan, B. J., Seegar, T. C. M., Dror, R. O., Kruse, A. C. & Blacklow, S. C. (2016). Crystal structure of a full-length human tetraspanin reveals a cholesterol-binding pocket. *Cell*, *167*(4), 1041–1051.e11. https://doi.org/10.1016/j.cell.2016.09.056.
27. Benedikter, B. J., Bouwman, F. G., Vajen, T., Heinzmann, A. C. A., Grauls, G., Mariman, E. C., Wouters, E. F. M., Savelkoul, P. H., Lopez-Iglesias, C., Koenen, R. R., Rohde, G. G. U. & Stassen, F. R. M. (2017). Ultrafiltration combined with size exclusion chromatography efficiently isolates extracellular vesicles from cell culture media for compositional and functional studies. *Science Reports*, *7*(1), 1–13. https://doi.org/10.1038/s41598-017-15717-7.
28. Vergauwen, G., Dhondt, B., Van Deun, J., De Smedt, E., Berx, G., Timmerman, E., Gevaert, K., Miinalainen, I., Cocquyt, V., Braems, G., Van Den Broecke, R., Denys, H., De Wever, O. & Hendrix, A. (2017). Confounding factors of ultrafiltration and protein analysis in extracellular vesicle research. *Science Reports*, *7*(1), 1–12. https://doi.org/10.1038/s41598-017-02599-y.
29. Kakarla, R., Hur, J., Kim, Y. J., Kim, J. & Chwae, Y. J. (2020). Apoptotic cell-derived exosomes: Messages from dying cells. *Experimental and Molecular Medicine*, *52*(1), 1–6. https://doi.org/10.1038/s12276-019-0362-8.
30. Crescitelli, R., Lässer, C., Szabó, T. G., Kittel, A., Eldh, M., Dianzani, I., Buzás, E. I. & Lötvall, J. (2013). Distinct RNA profiles in subpopulations of extracellular vesicles: Apoptotic bodies, microvesicles and exosomes. *Journal of Extracellular Vesicles*, *2*(1). https://doi.org/10.3402/jev.v2i0.20677.
31. Guerreiro, E. M., Vestad, B., Steffensen, L. A., Aass, H. C. D., Saeed, M., Øvstebø, R., Costea, D. E., Galtung, H. K. & Søland, T. M. (2018). Efficient extracellular vesicle isolation by combining cell media modifications, ultrafiltration, and size-exclusion chromatography. *PLoS One*, *13*(9), 1–17. https://doi.org/10.1371/journal.pone.0204276.
32. Costantini, L. M., Fossati, M., Francolini, M. & Snapp, E. L. (2012). Assessing the tendency of fluorescent proteins to oligomerize under physiologic conditions. *Traffic (Copenhagen, Denmark)*, *13*(5), 643–649. https://doi.org/10.1111/j.1600-0854.2012.01336.x.
33. Shaner, N. C., Steinbach, P. A. & Tsien, R. Y. (2005). A guide to choosing fluorescent proteins. *Nature Methods*, *2*(12), 905–909. https://doi.org/10.1038/nmeth819.
34. Kessler, R. J. & Fanestil, D. D. (1986). Interference by lipids in the determination of protein using bicinchoninic acid. *Analytical Biochemistry*, *159*(1), 138–142. https://doi.org/10.1016/0003-2697(86)90318-0.
35. Brown, R. E., Jarvis, K. L. & Hyland, K. J. (1989). Protein measurement using bicinchoninic acid: Elimination of interfering substances. *Analytical Biochemistry*, *180*(1), 136–139. https://doi.org/10.1016/0003-2697(89)90101-2.
36. Osteikoetxea, X., Balogh, A., Szabó-Taylor, K., Németh, A., Szabó, T. G., Pálóczi, K., Sódar, B., Kittel, Á., György, B., Pállinger, É., Matkó, J. & Buzás, E. I. (2015). Improved characterization of EV preparations based on protein to lipid ratio and lipid properties. *PLoS One*, *10*(3), 1–16. https://doi.org/10.1371/journal.pone.0121184.

SUPPORTING INFORMATION

Additional supporting information may be found in the online version of the article at the publisher's website.

How to cite this article: Sanchez, B. C., Hinchliffe, M., & Bracewell, D. G (2022). GFP-tagging of extracellular vesicles for rapid process development. *Biotechnology Journal*, e2100583. https://doi.org/10.1002/biot.202100583